# Zinc Phthalocyanine Tetrasulfonate-Loaded Ag@mSiO$_2$ Nanoparticles for Active Targeted Photodynamic Therapy of Colorectal Cancer

*Hanieh Montaseri\*, Nokuphila Winifred Nompumelelo Simelane and Heidi Abrahamse*

*Laser Research Centre, Faculty of Health Sciences, University of Johannesburg, Doornfontein, South Africa*

Colorectal cancer has high morbidity and mortality rate, with a high level of metastasis and recurrence due to the poor therapeutic effects. Photodynamic therapy (PDT) as an emerging clinical modality for cancer treatment provides remarkable advantages over existing treatments by generating reactive oxygen species (ROS) through light irradiating photosensitizers (PSs) in the presence of oxygen. PDT can induce immunity against recurrence and destruction of metastases. The application of nanoparticles (NPs) in targeted cancer therapy is coming to light to circumvent the limitations associated with low physiological solubility and lack of selectivity of the PS towards tumor sites. In this *in vitro* study, we proved the added value of NP systems on PS efficacy and a tumor-targeting ligand. Using core/shell Ag@mSiO$_2$ NPs loaded with ZnPcS$_4$ PS and folic acid (FA), stronger cellular localization in the human colorectal cancer cell line (Caco-2) was observed compared to the passive NC and free PS. Additionally, light-induced photodynamic activation of the ZnPcS$_4$/Ag@mSiO$_2$-FA nanoconjugate (NC) elicited a strong cytotoxicity effect mediated by post-PDT. The results also revealed that the active NC was able to decrease the cell viability remarkably to 38.0% ± 4.2 *** compared to the passive NC (67.0% ± 7.4*) under 0.125 μM ZnPcS$_4$ (IC$_{50}$). More importantly, the actively targeted NC-induced apoptosis where cell cycle analysis elaborated on cell death through the G0 phase, indicating the final NC's efficacy 20 hr post-PDT treatment.

Keywords: colorectal cancer, Ag@mSiO2 nanoparticles, photodynamic therapy, ZnPcS4 photosensitizer, targeted therapy

## 1 INTRODUCTION

Colorectal cancer (CRC) is the third most common cancer that results from the cumulation of genetic and epigenetic modifications and alterations. An overall survival rate of 50% after surgical treatment has been reported for the patients with CRC, while half of them experience recurrence (Hani et al., 2021). The major tumor progression factors include smoking, improper diet, and lack of physical activities together with cytokines, growth factors, and certain chemicals (Huryn et al., 2019). The conventional curative therapies for CRC are chemotherapy, radiotherapy, and surgery. However, the resistance of tumor cells to chemo drugs, and their detrimental side effects with high toxicity on healthy cells, necessitates other treatment modalities to eradicate the primary tumors.

Photodynamic therapy (PDT) is a clinically approved, non-invasive therapeutic modality that involves the utilization of a photosensitizer (PS) followed by irradiation at a specific wavelength of light (Agostinis et al., 2011). Clinical studies showed that PDT can cure early-stage tumors, and can be incorporated into the mainstream cancer treatment (Agostinis et al., 2011). Three essential components required for PDT consist of PS, light, and oxygen. They can generate a photochemical reaction that facilitates the production of a highly reactive product termed singlet oxygen species (ROS).

PDT can induce cell death through apoptosis, necrosis, or autophagy pathways. Necrotic cell death or accidental cell death is triggered when high fluency and PS concentrations are applied, accompanied by disruption of the plasma membrane and organelles and swelling of the cytoplasm (Lucky et al., 2015). However, it is not the preferred mode of cell death following PDT as it can cause inflammatory responses due to the release of the intracellular contents into the extracellular environment (Melamed et al., 2015). Cell death described after PDT is usually through apoptosis and involves membrane blebbing, nuclear fragmentation, and other distinctive changes such as cell shrinkage and the formation of apoptotic bodies that are scavenged by phagocytes, thereby preventing an inflammatory response (Almeida et al., 2004; Bretin et al., 2019).

Photodamage based on PDT hinges on the type of PS, its localization, light dose, and cell genotype. Currently, most clinical and pre-clinical PSs are hydrophobic with a high tendency for aggregation in aqueous media, thereby reducing the photosensitizing efficacy (Simioni et al., 2006).

It should be borne in mind that hydrophobic/hydrophilic properties, charge, and protein-binding affinity of the PS or NCs can affect their subcellular localization. Hydrophobic PSs tend to be localized in the endoplasmic reticulum and cell membrane, while hydrophilic PSs accumulate in the lysosome. However, both water- and lipid-rich moieties can uptake amphiphilic PSs. In this sense, zinc phthalocyanine tetrasulfonate ($ZnPcS_4$) as an amphiphilic PS has been designed to circumvent the issue associated with aggregation. $ZnPcS_4$ has an intensive absorption in the red region with high singlet and triplet oxygen production (Gantchev et al., 2005). Furthermore, it provides high cellular localization, efficient depth penetration of light (Portilho et al., 2013), and subcellular organelle targeting due to its effective diffusion through the cell membrane (Banfi et al., 2007).

A study noted that phthalocyanine complexes such as anionic $ZnPcS_4$ can efficiently bind to phospholipid membranes through metal–phosphate coordination (Dhami et al., 1996). The nanostructured photosensitive molecular structure can also minimize the aggregation tendency and release the PSs to the targeted tissue (Sibata et al., 2000). They can spontaneously accumulate in tumors through an enhanced permeability and retention (EPR) effect or active targeting moieties.

Aiming to potentialize the efficacy of PDT on colon cancer while using nanostructured drug delivery systems loading PSs, we reported on the fabrication of core/shell silver-mesoporous silica ($Ag@mSiO_2$) NPs which were loaded with $ZnPcS_4$ PS and conjugated to folic acid (FA) for PDT of Caco-2 cancer cells.

Larger enhanced-absorption cross-sections together with higher photostability with minimal photobleaching of metal NPs relative to photo-absorbing dyes have made them ideal candidates for efficient laser therapy (Huang et al., 2008). Additionally, mesoporous silica NPs provide high surface area and pore volume, resulting in high loading efficiency of the PSs. They can also protect the PSs from aggregation and control the PS release in the cancer tissue, consequently reducing the overall PS dosage and adverse side effects (Zhao et al., 2009; Krajczewski et al., 2019). Easy functionalization of the surface of mesoporous silica NPs with various targeting agents and biomolecules is an imperative property in drug delivery (Porrang et al., 2022). On the other hand, FA is a water-soluble vitamin B in which the low folate diet is linked to some malignancies such as colon cancer (Fife et al., 2011). Folate receptors are overexpressed in colorectal carcinomas where their high affinity for FA is maintained when FA is bound to folate-linked drugs or NPs (El-Hammadi et al., 2017).
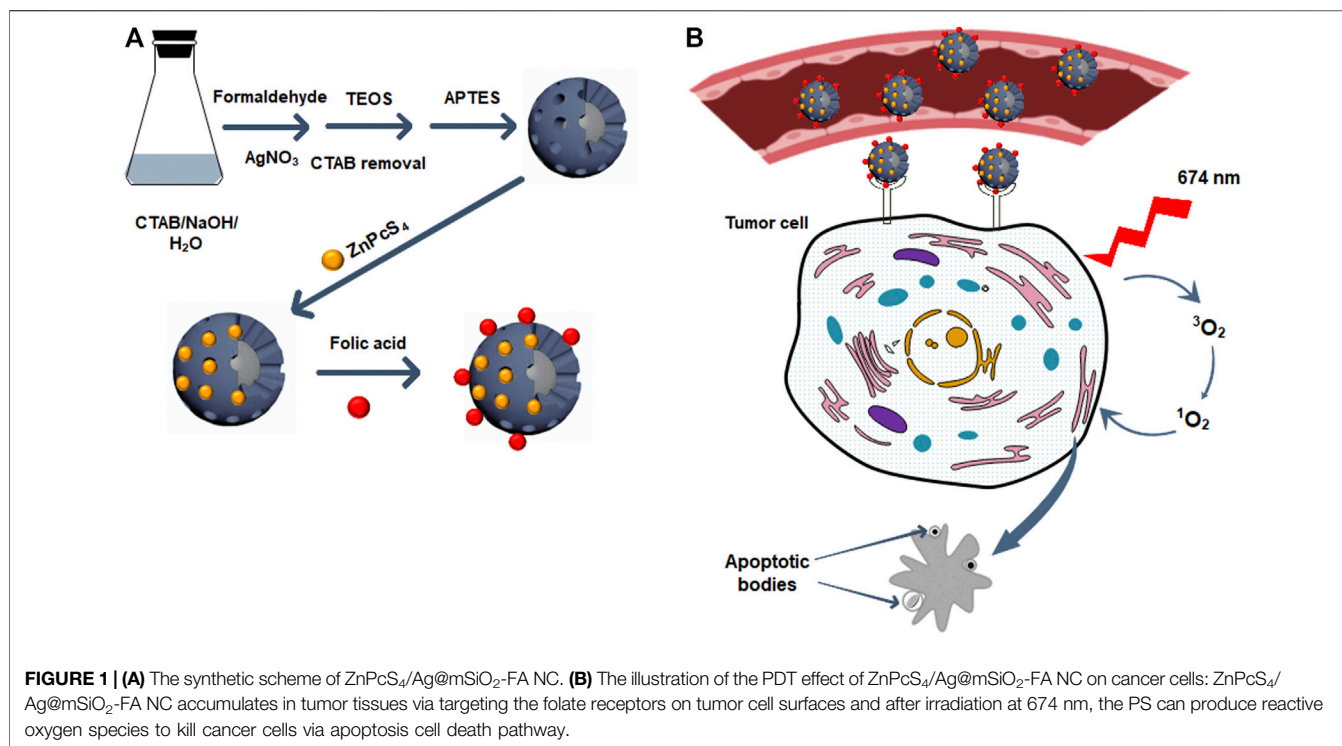
# 2 MATERIALS AND METHODS

## 2.1 Materials

Zinc phthalocyanine tetrasulfonate ($ZnPcS_4$) was purchased from Santa Cruz Biotechnology, Inc (Santa Cruz®: sc-264509A). Phosphate-buffered saline (PBS, 10× concentrate), SH-PEG$_{2k}$-NH$_2$ (HCl salt, average Mn 2,000), tri-sodium citrate (for molecular biology, ≥ 99%), dimethyl sulfoxide (DMSO, anhydrous, ≥ 99.9%), N-ethyl-N′-(3-dimethylaminopropyl) carbodiimide (EDC, BioXtra), N-hydroxysuccinimide (NHS, 98%), tannic acid (ACS reagent), folic acid (FA, ≥ 97%), silver nitrate ($AgNO_3$, ACS reagent, ≥ 99.0%), formaldehyde (for molecular biology, 36.5–38% in $H_2O$), tetraethyl orthosilicate (TEOS, reagent grade), 3-aminopropyltriethoxysilane (APTES, 99%), hexadecyltrimethylammonium bromide (CTAB, > 99%), and sodium hydroxide (NaOH, BioXtra, ≥ 98%) were purchased from Sigma Aldrich. Analytical grade chemicals and reagents as well as Millipore water were used throughout this study. All glassware was washed thoroughly with aqua regia solution.

## 2.2 Fabrication of $ZnPcS_4$/Ag@ mSiO$_2$-FA NC

A facile one-pot process was utilized for the preparation of the core/shell $Ag@mSiO_2$ (Han et al., 2011; Wijesiri et al., 2018). A solution containing 20 mg CTAB, 240 μL NaOH (0.5 M), and 9.8 ml Millipore water was prepared and stirred at 80°C for 10 min. Afterward, 60 μL formaldehyde was added dropwise to the solution followed by the addition of 240 μL silver nitrate (0.1 M) and 80 μL TEOS and stirred at 80°C for 2 hr. Anhydrous ethanol was used to wash the resultant NPs. To remove the CTAB surfactant and form porous NPs, they were dispersed in $NH_4NO_3$ (6 mg/ml) ethanol solution and reacted at 60°C for 30 min under vigorous stirring followed by several steps of Millipore water washing. Functionalizing the NPs with amino groups was performed by dissolving the precipitate in ethanol and 20 μL APTES was added and stirred at 60°C for 2 hr. The prepared Ag@

FIGURE 1 | (A) The synthetic scheme of ZnPcS$_4$/Ag@mSiO$_2$-FA NC. (B) The illustration of the PDT effect of ZnPcS$_4$/Ag@mSiO$_2$-FA NC on cancer cells: ZnPcS$_4$/Ag@mSiO$_2$-FA NC accumulates in tumor tissues via targeting the folate receptors on tumor cell surfaces and after irradiation at 674 nm, the PS can produce reactive oxygen species to kill cancer cells via apoptosis cell death pathway.

mSiO$_2$-NH$_2$ NPs were washed and centrifuged with ethanol several times and dispersed in Millipore water (**Figure 1A**).

To load ZnPcS$_4$ PS into Ag@mSiO$_2$-NH$_2$ NPs, 1 ml of the PS was dispersed in 1 ml of the NPs and agitated overnight in the dark. A mixture of ethanol/water (1:1) was used to remove the excess ZnPcS$_4$ and centrifuged at 15,000 rpm followed by dispersing the prepared ZnPcS$_4$/Ag@mSiO$_2$-NH$_2$ NC in PBS (**Figure 1A**).

Conjugation of FA to the ZnPcS$_4$/Ag@mSiO$_2$-NH$_2$ NC was carried out by activation of the carboxyl groups of FA via EDC/NHS reactions. Therefore, 20 mg FA in DMSO was mixed with 100 mg EDC and 100 mg NHS for 24 hr. Ice-cold acetone was utilized to remove dicyclohexylurea as a by-product. The pellet was then dissolved in a mixture of DMSO: PBS and mixed with 1 ml ZnPcS$_4$/Ag@mSiO$_2$-NH$_2$ NC with continuous stirring for 1 hr in the dark. The resulting ZnPcS$_4$/Ag@mSiO$_2$-FA NC was then purified with centrifugation to remove the excess FA and dispersed in PBS (**Figure 1A**).

## 2.3 In Vitro Cell Line Models

Human colon cancer cells (CaCo-2 Cellonex Cat SS1402 CCAC-FL; CCAC-C) were obtained from the American Type Culture Collection. Caco-2 cells were seeded in DMEM media, containing 10% fetal bovine serum (FBS), 100 U penicillin and 100 μg/ml streptomycin solution, 2.5 μg/ml amphotericin B, 1 mM sodium pyruvate, and 2 mM L-glutamine and incubated at 37°C in 5% CO$_2$ with 85% humidified air. The cells were then seeded at a seeding amount of 6×10$^5$ cells/3 ml in 3.4-cm diameter culture plates and maintained for 24 hr for cellular attachment before conducting *in vitro* cellular experiments and flow cytometry for PDT.

WS1 human skin fibroblasts were received from the American Type Culture Collection (ATTC CRL-1502). The cells were seeded in MEM media, enriched with 10% FBS, 1 mM sodium pyruvate, 0.1 mM nonessential amino acids, 2 mM L-glutamine, 2.5 μg/ml amphotericin B, 100 U penicillin, and 100 μg/ml streptomycin solution at 37°C in 5% CO$_2$ and 85% humidity. The cells were cultured at the same seeding amount as the Caco-2 cells in complete cell culture media and were used for flow cytometry assays as a control to compare the effect of final NC-PDT on normal cells.

## 2.4 Cellular Uptake of ZnPcS$_4$/Ag@mSiO$_2$-FA by Live Imaging Microscope

The intracellular localization of the NCs was determined based on the described protocol (Montaseri et al., 2021; Simelane et al., 2021). Briefly, Caco-2 cells were seeded on sterilized coverslips at a density of 3.0×10$^5$ cells in 1 ml media and cultured for 24 hr. Subsequently, the media was replaced with fresh media, and the cells were treated with the NCs at an equivalent ZnPcS$_4$ concentration of 0.125 μM. After removal of the media, the cells were washed with PBS three times, fixed with 4% formaldehyde, and permeabilized with a solution containing 0.5% Triton X-100. The cells were then counterstained with 4′, 6-diamidino-2-phenylindole (DAPI) in the dark and observed by a live imaging microscope (Carl Zeiss Axio Observer Z1).

## 2.5 In Vitro Photodynamic Effect of ZnPcS$_4$/Ag@mSiO$_2$-FA

The cells were first seeded at a density of 3.0 × 10$^5$ cells in complete media. After 24 hr post-incubation, the media was

replaced by fresh media containing NCs at different concentrations as previously established in our group (Simelane et al., 2021). The experimental groups were divided into two subgroups, with and without 674 nm laser irradiation with a semiconductor diode laser (10 J/cm$^2$, 9.5 mW/cm$^2$, 17 min). The cells were then incubated for another 20 hr for cellular experiments. ZnPcS$_4$/Ag@mSiO$_2$ NC was considered a passive targeting nanosystem. The cells in culture media or a mixture of media and NPs alone were assessed as control groups. All experiments were performed in the dark at room temperature to eliminate any light reflection.

## 2.6 Photodynamic Cellular Experiments

### 2.6.1 LDH Cytotoxicity Test

Cellular cytotoxicity was measured after 20 hr post PDT treatment by the amount of lactate dehydrogenase (LDH) in culture media as dead cells release LDH from their damaged membrane. The release of LDH was measured at 490 nm using the CytoTox96® Non-Radioactive Cytotoxicity Assay (Promega, G1780) based on the manufacturer's instructions by the VICTOR Nivo® multimode plate reader (PerkinElmer, HH35940080 EN) and compared with the positive control indicative of 100% cytotoxicity.

### 2.6.2 ATP Cell Viability Test

CellTiter-Glo® ATP luminescence assay (Promega, G7570) was established to quantify the number of adenosine triphosphate (ATP) produced by metabolically active cells according to the manufacturer's instructions. This assay results in the production of a luminescent signal that corresponds to the amount of ATP present. The luminescent signal of the cells in relative light units (RLUs) was measured by the VICTOR Nivo® multimode plate reader (PerkinElmer, HH35940080 EN). ATP viability assay was performed three times and presented as a percentage relative to the cells only (control).

## 2.7 Hoechst DNA Damage Test

Bisbenzimide derivate fluorescent stain or Hoechst 33258 was used to detect cellular nuclear DNA damage. The chromatin state of the cell and DNA conformation can determine the degree of nuclear damage and the Hoechst stain can distinguish live, apoptotic, or necrotic cell death pathways. Therefore, to confirm the PDT effect of the NCs, Caco-2 cells were seeded on sterile coverslips and incubated at 37°C to allow for cellular attachment. After 24 hr, the cells were subjected to an equivalent concentration of ZnPcS$_4$ in the NCs and were divided into treated and nontreated groups whereby the treated groups were irradiated at a 10 J/cm$^2$ dose. After 20 hr post-irradiation, the culture plates were rinsed with ice-cold PBS and fixed to the coverslips with a 3.7% (v/v) formaldehyde solution. The cells were then stained with 1.0 μg/ml Hoechst 33258 fluorescent dye. A fluorescent microscope with the 358Ex/461 Em DAPI filter was used to detect the blue fluorescence of the stain. All experiments were conducted with minimum light exposure to reduce photobleaching of the PS or the stains.

## 2.8 Apoptosis and Necrosis Analysis by Flow Cytometry

The treated cells with the NCs with or without light irradiation were stained 20 hr post-PDT via fluorescein isothiocyanate (FITC) annexin V/propidium iodide (PI) cell death detection kits (BD Scientific: BD/556570), following the manufacturer's instructions. This assay evaluates the percentage of cells undergoing early or late apoptotic, as well as necrotic cell death, phases. The stained cells were then analyzed using the BD Accuri™ C6 flow cytometer, BD Life Sciences, San Jose, CA, United States.

## 2.9 Cell Cycle Analysis

The control and experimental treated cells were subjected to cell cycle analysis using flow cytometry 20 hrs post-PDT. Cells were trypsinized and fixed in cold 70% ethanol for 30 min. The cells were then washed with PBS and treated with a mixture of 50 μL RNase (100 μg/ml) and 200 μL propidium iodide (PI, 50 μg/ml). The stained cells were used for the analysis using a flow cytometer.

## 2.10 Statistical Analysis

Biochemical assays were performed in triplicate, and standard deviation was reported by error bars. Student's t-test and one-way ANOVA as statistical analyses were applied in the 95% confidence interval ($p < 0.05^*$, $p < 0.01^{**}$, or $p < 0.001^{***}$) to compare the significant difference between control and experimental groups.
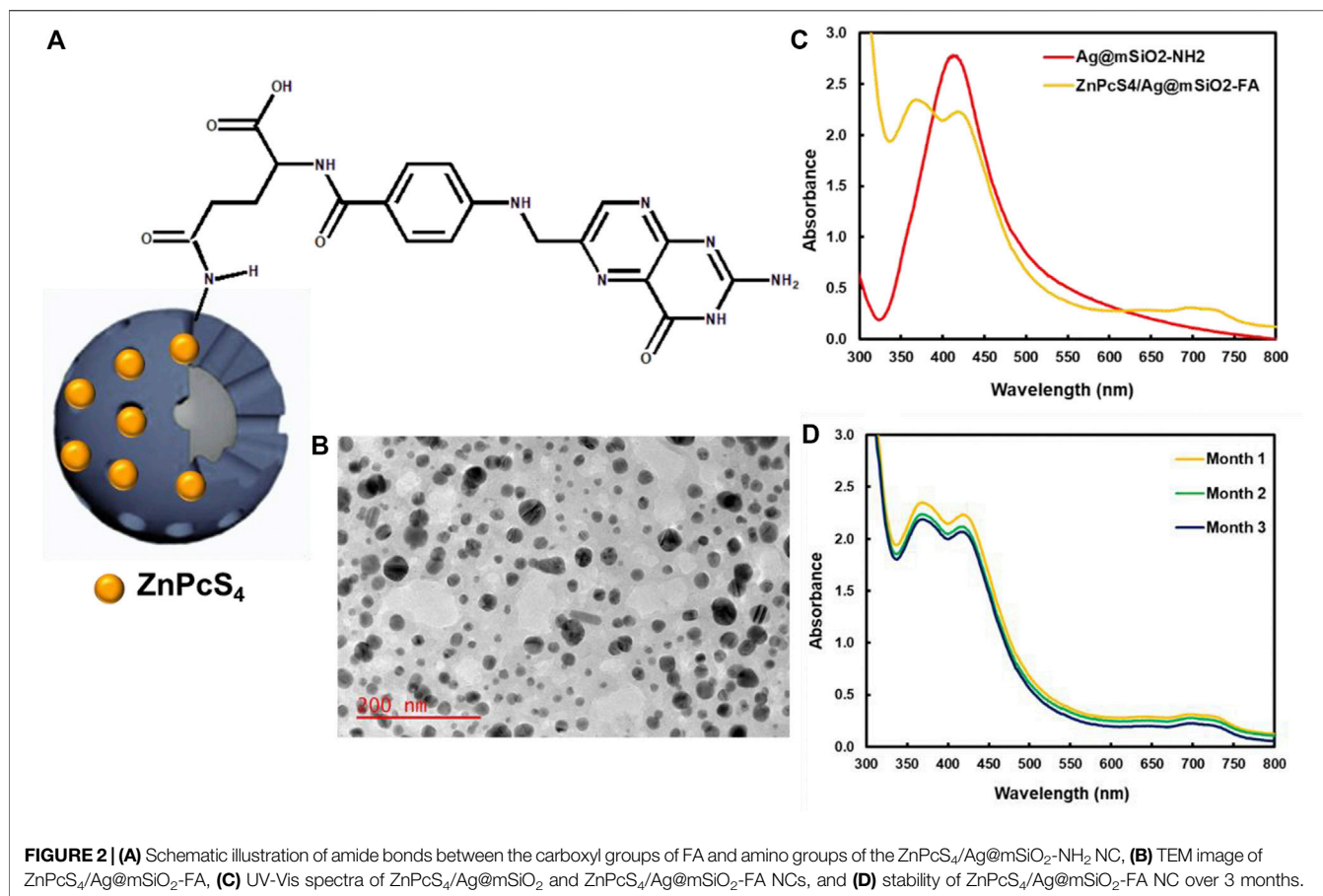
## 3 RESULTS AND DISCUSSION

### 3.1 Fabrication and Characterization of ZnPcS$_4$/Ag@mSiO$_2$-FA

The design and synthesis of ZnPcS$_4$/Ag@mSiO$_2$-FA are illustrated in **Figures 1A,B** elucidates the PDT effect of ZnPcS$_4$/Ag@mSiO$_2$-FA NC. ZnPcS$_4$/Ag@mSiO$_2$-FA NC was synthesized and characterized where hydrogen bonding and electrostatic interactions between the amino groups of silica and sulfonate groups of ZnPcS$_4$ were responsible for maintaining the PS inside the mesoporous silica shells. FA as an active targeting ligand was then integrated through EDC/NHS reaction to form amide bonds between the carboxyl groups of FA and amino groups of the ZnPcS$_4$/Ag@mSiO$_2$-NH$_2$ (**Figure 2A**). These amide bonds are formed by a simple chemical reaction. In the presence of EDC, the α-COOH group of FA converts to a more reactive NHS group (succinimide group) which then reacts with the primary NH$_2$ group of the NPs (El-Hammadi et al., 2017). However, this conjugation does not interfere with the ability of FA to bind to folate receptors as the folate moieties are located on the surface when the NCs are produced (Sudimack and Lee, 2000; Low and Kularatne, 2009).

The physicochemical properties of the Ag@mSiO$_2$ NPs comprised a mean diameter of 24.0 ± 6.2 nm by TEM analysis for the silver core with the fiber-like network for the silica shell (**Figure 2B**). A polydispersity index of 0.45 ± 0.02 and 0.37 ± 0.04 was found for the ZnPcS$_4$/Ag@mSiO$_2$ and ZnPcS$_4$/Ag@mSiO$_2$-FA NCs, respectively, which proved their great size distribution with no aggregation (Danaei et al., 2018).

**Figure 2C** illustrates UV-Vis absorption spectra of Ag@mSiO$_2$-NH$_2$ NPs and ZnPcS$_4$/Ag@mSiO$_2$-FA NC. A noticeable

**FIGURE 2 | (A)** Schematic illustration of amide bonds between the carboxyl groups of FA and amino groups of the ZnPcS$_4$/Ag@mSiO$_2$-NH$_2$ NC, **(B)** TEM image of ZnPcS$_4$/Ag@mSiO$_2$-FA, **(C)** UV-Vis spectra of ZnPcS$_4$/Ag@mSiO$_2$ and ZnPcS$_4$/Ag@mSiO$_2$-FA NCs, and **(D)** stability of ZnPcS$_4$/Ag@mSiO$_2$-FA NC over 3 months.

localized surface plasmon resonance (LSPR) absorption band at ~412 nm was related to the Ag@mSiO$_2$-NH$_2$ NPs, while an absorption peak at 674 nm showed the presence of ZnPcS$_4$ PS and a peak at 365 nm represented the successful formation of amide bonds between amino groups of Ag@mSiO$_2$-NH$_2$ NPs and carboxyl groups of FA.

Photostability of the final actively targeted ZnPcS$_4$/Ag@mSiO$_2$-FA NC in PBS over 3 months is shown in **Figure 2D**. No remarkable changes were observed in Q bands of the PS at 674 nm or the LSPR peak of the NPs, indicating high stability of the NC with no aggregation. However, a decrease in the electron density of the NC caused a slight decline in the LSPR peak of the ZnPcS$_4$/Ag@mSiO$_2$-FA (Hoener et al., 2017). It is worth mentioning that poor solubility of small NPs in aqueous media or changing of the surface polarity/charge upon adsorption of molecules are attributed to their easy aggregation (Wang N. et al., 2019). It is therefore surface coating (e.g., silica coating) is applied to not only reduce the aggregation but also to enhance the stability of nanocarriers and facilitate drug loading (Yang et al., 2009; Wang N. et al., 2019).

A zeta potential of $-15.0 \pm 0.8$ and $-14.4 \pm 0.6$ was achieved for the ZnPcS$_4$/Ag@mSiO$_2$ and ZnPcS$_4$/Ag@mSiO$_2$-FA NCs, respectively, which based on modeling and tumor cylindroid studies, can easily penetrate deeply into the tumor (Kim et al., 2010; Kievit and Zhang, 2011).

The loading amount of the PS in the ZnPcS$_4$/Ag@mSiO$_2$ and ZnPcS$_4$/Ag@mSiO$_2$-FA based on the regression equation was estimated to be 21.8 and 22.3 µM, respectively.

## 3.2 Subcellular Localization of the NCs

The subcellular uptake efficiency of active FA-attached NC and passive NC (ZnPcS$_4$/Ag@mSiO$_2$) was evaluated in Caco-2 cells *in vitro* (**Figure 3**). Uptake of the actively targeted folate-NC under 0.125 µM ZnPcS$_4$ was easily observed, whereas the signal was significantly lower for passive NC and the PS alone. These observations confirmed that the actively targeted NC could recognize receptors overexpressed on Caco-2 cells and provide higher cellular uptake relative to the passive NC (**Figure 1B**). Hence, no off-target specific uptake occurred. Generally, the folate receptor is overexpressed on the surface of many cancer cells as they require folic acid for DNA biosynthesis and DNA repair (Kievit and Zhang, 2011).

## 3.3 Photodynamic Effect of the NCs on Caco-2 Cells

The morphological changes of Caco-2 cells under PDT were visualized using a light inverted microscope at 100X magnification with a digital camera (**Figure 4A**). Administration of the Ag@mSiO$_2$ NPs or the NCs (non-
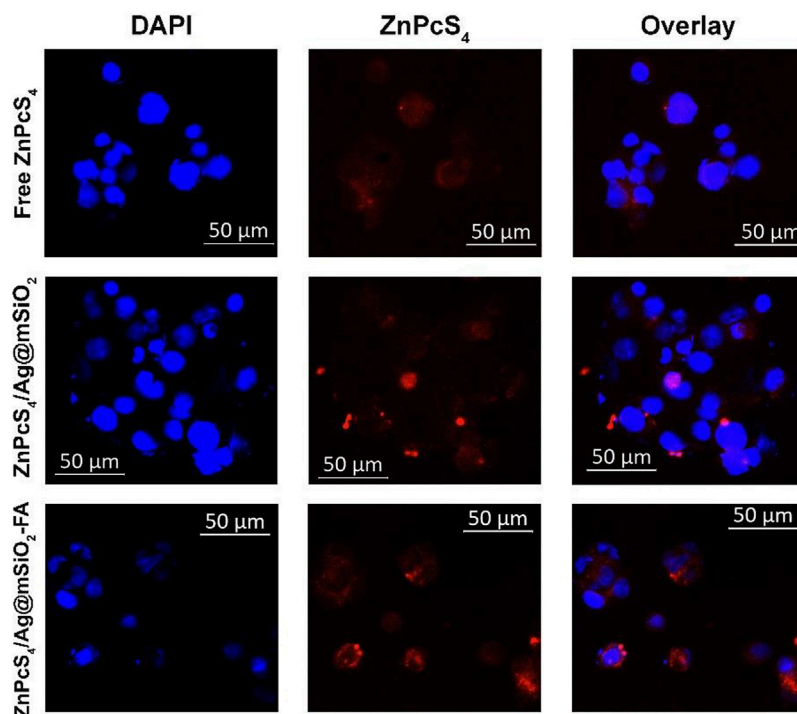
**FIGURE 3 |** Subcellular localization of passive and actively targeted NCs in Caco-2 cells. Blue fluorescence is indicative of DAPI-stained nuclei and red autofluorescence shows the localization of the PS or the NCs.

irradiated/untreated control groups) showed normal morphology with intact cellular structures and undamaged nuclei. However, Caco-2 cells submitted to the passive $ZnPcS_4/Ag@mSiO_2$ or active $ZnPcS_4/Ag@mSiO_2$-FA NCs under PDT exhibited a breakdown of the intercellular structure and more importantly, the cells treated with the actively targeted NC exhibited hallmarks of apoptosis such as cell shrinkage, nuclear chromatin condensation, and the formation of phagocytic vesicles.
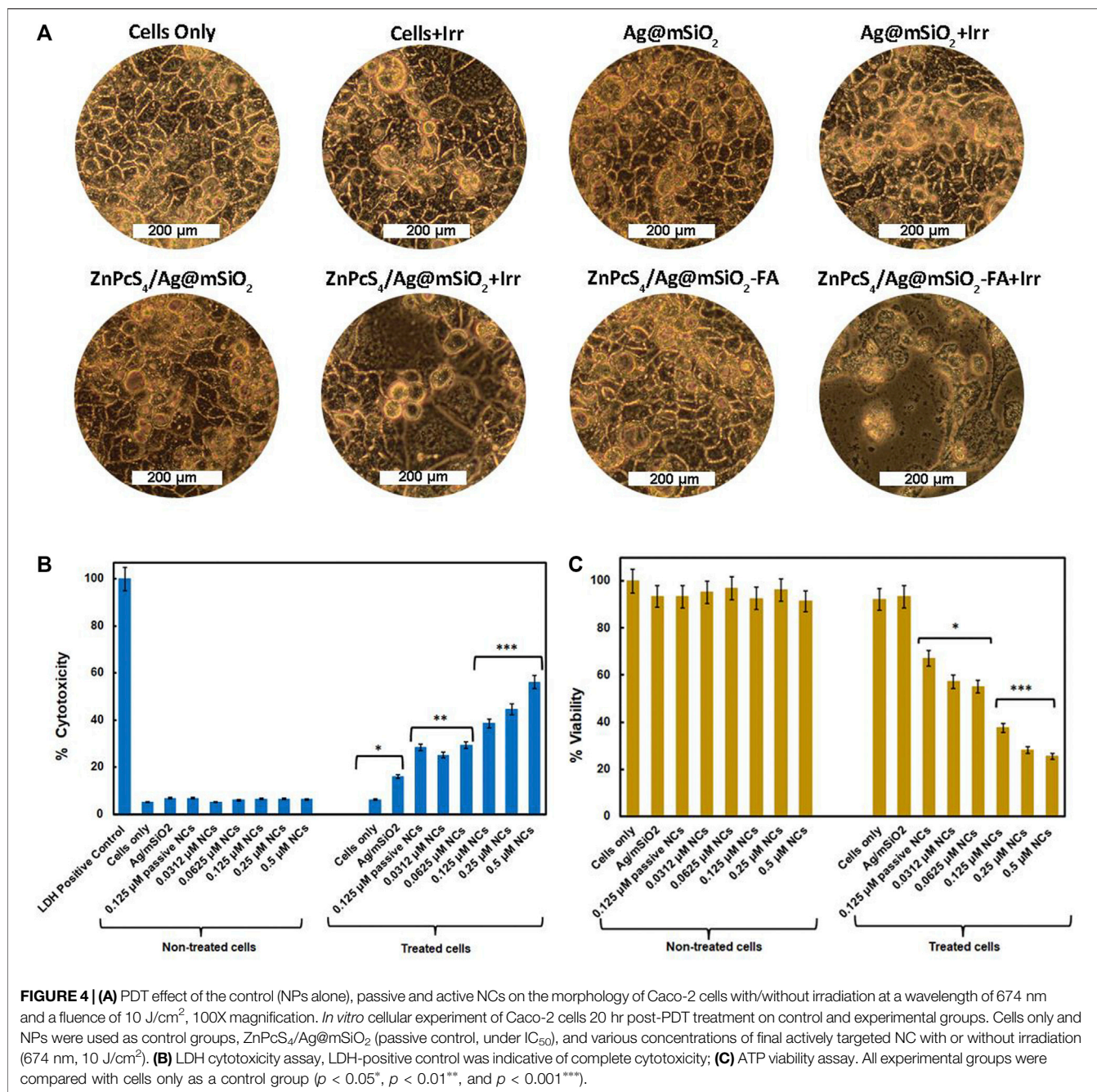
As demonstrated in **Figure 4B**, unloaded NPs and NCs with no irradiation exhibited negligible cytotoxicity confirming their adequate biocompatibility and safety for Caco-2 treatment. However, the cytotoxic effect of the FA-decorated NC under light irradiation increased in a dose-dependent manner. Moreover, the actively targeted NC showed additional cytotoxicity ($38.5\% \pm 0.57^{***}$) compared to the passive NC ($28.5\% \pm 0.35^{**}$) under an equivalent concentration of $0.125\,\mu M$ ($IC_{50}$) proving enhanced cellular localization via folate receptor-mediated endocytosis.

Figure 4C displays the cell viability of the Caco-2 cells treated with different concentrations of the active NC, the unloaded NPs, and $ZnPcS_4/Ag@mSiO_2$ NC ($0.125\,\mu M$, passive control). No notable differences were detected in viability for the cell treated with either unloaded NPs, passive or active targeted NCs with no light irradiation which was in agreement with the LDH cell cytotoxicity. Whereas the cells received various concentrations of the active NC followed by irradiation resulting in cell viability inhibition with increasing doses of $ZnPcS_4$. Additionally, under the $IC_{50}$ value of $ZnPcS_4$ ($0.125\,\mu M$) with

a light dose of $10\,J/cm^2$, $ZnPcS_4/Ag@mSiO_2$-FA could reduce the cell viability to $38.0\% \pm 4.2^{***}$ relative to $ZnPcS_4/Ag@mSiO_2$ with $67.0\% \pm 7.4^*$ viability and the $IC_{50}$ for FA loaded NC was found to be $0.0625\,\mu M$ which was 2-fold less than free $ZnPcS_4$ PS ($0.125\,\mu M$) in the previous study (Simelane et al., 2021). The higher cell viability in passive $ZnPcS_4/Ag@mSiO_2$ NC compared to free $ZnPcS_4$ might be attributed to the faster entry of free PS into the cells (Wang Y. et al., 2019).

## 3.4 Nuclear DNA Damage Analysis

Hoechst nuclear stain was utilized to evaluate the level of DNA damage (**Figure 5**). It emits blue fluorescence when it binds to DNA that can be used to assess apoptosis. Control groups of cells only and irradiated cells illustrated a perfectly dense spherical nucleus with negligible damage. The cells were treated with the NCs with no irradiation and also showed a spherical homogenously stained nucleus, while irregular and scattered nuclear shape was observed for the treated cells with the $ZnPcS_4/Ag@mSiO_2$-FA NC and irradiated at 674 nm suggesting nuclear and DNA chromatin fragmentation. In the case of treatment with passive $ZnPcS_4/Ag@mSiO_2$ NC, cellular nuclei started changing in shape, and very slight fragmentation was observed (shown with arrows) in comparison to the actively targeted NC. These results suggest that the $ZnPcS_4/Ag@mSiO_2$-FA NC could induce apoptosis for the treated cells under PDT (PS/irradiation). We also performed Annexin V-FITC/PI double staining experiment to identify the apoptosis rate of cells where the results for the NCs were consistent with the Hoechst DNA damage analysis.

**FIGURE 4 | (A)** PDT effect of the control (NPs alone), passive and active NCs on the morphology of Caco-2 cells with/without irradiation at a wavelength of 674 nm and a fluence of 10 J/cm$^2$, 100X magnification. *In vitro* cellular experiment of Caco-2 cells 20 hr post-PDT treatment on control and experimental groups. Cells only and NPs were used as control groups, ZnPcS$_4$/Ag@mSiO$_2$ (passive control, under IC$_{50}$), and various concentrations of final actively targeted NC with or without irradiation (674 nm, 10 J/cm$^2$). **(B)** LDH cytotoxicity assay, LDH-positive control was indicative of complete cytotoxicity; **(C)** ATP viability assay. All experimental groups were compared with cells only as a control group ($p < 0.05^*$, $p < 0.01^{**}$, and $p < 0.001^{***}$).

## 3.5 Detection of Apoptosis and Necrosis

Caco-2 cells were treated with the passive and actively targeted NCs under an equivalent concentration of ZnPcS$_4$ and were analyzed by flow cytometry (**Figure 6**). The photodynamic therapeutic effect of the NCs on WS1 fibroblast cells was also investigated to clarify the PDT effect of the NCs on normal cells. As illustrated in **Figure 6**, control, passive, and active NC treated cells with no light irradiation were mostly viable and they did not induce cell death (live cells >90%), whereas the rate of early and late apoptosis treated cells with the passive and active NCs in the presence of light irradiation significantly increased to 44.0% ±

1.6** and 52.4% ± 3.5**, respectively. Therefore, apoptosis was certainly the main death mechanism by the NCs-PDT. Moreover, the highest percentage of apoptotic cells (52.4% ± 3.5**) was reported for the actively targeted ZnPcS$_4$/Ag@mSiO$_2$-FA NC suggesting an enhanced cellular localization via folate-receptor–mediated endocytosis resulting in a remarkable PDT effect against the Caco-2 cells. In sharp contrast, both NCs exhibited a negligible photodynamic therapeutic effect on WS1 cells, and based on the apoptotic ratio cells, it can be assumed that the NCs presented adequate biocompatibility and safety with minimal side effects on normal cells.
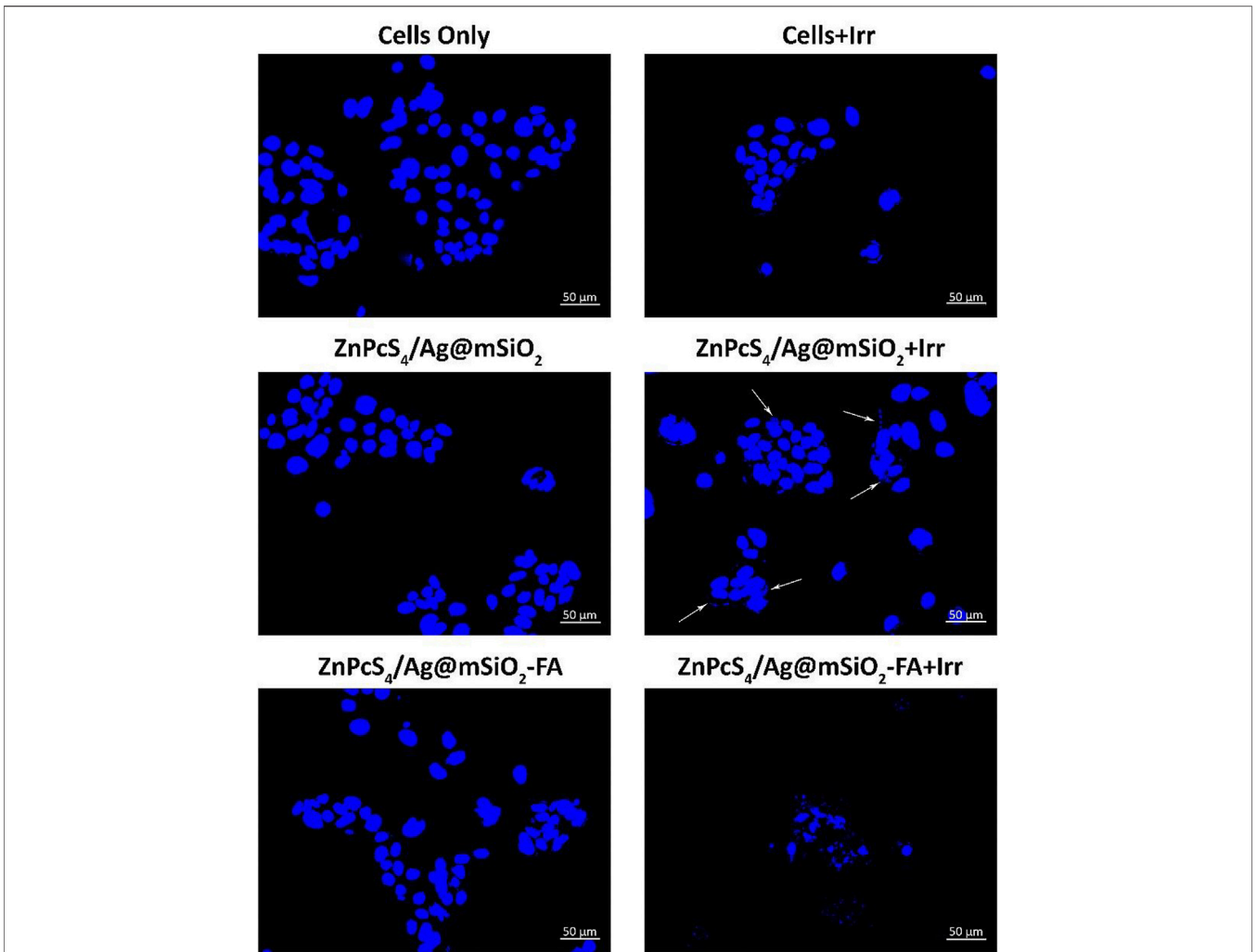
**FIGURE 5 |** Hoechst 33258 Caco-2 cells nuclear DNA damage with the passive and final actively targeted NCs.
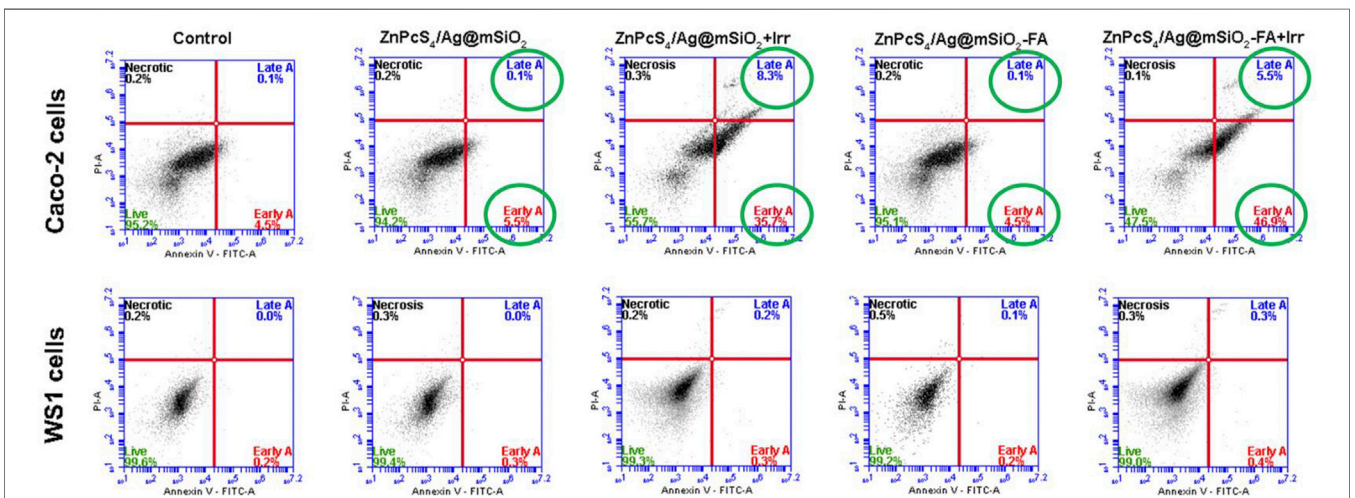


**FIGURE 6 |** Annexin V-FITC/PI cell death analysis of Caco-2 and WS1 cells using flow cytometry, 20 hr post-irradiation with passive and actively targeted NCs under the equivalent concentration of ZnPcS$_4$ (0.125 µM, 10 J/cm$^2$ fluency). Cells with no treatment (PS/irradiation) were used as a control.

**FIGURE 7 |** Cell cycle analysis via DNA quantification using flow cytometry on Caco-2 cells with passive and actively targeted NCs under an equivalent concentration of ZnPcS$_4$ and 10 J/cm$^2$ fluency.
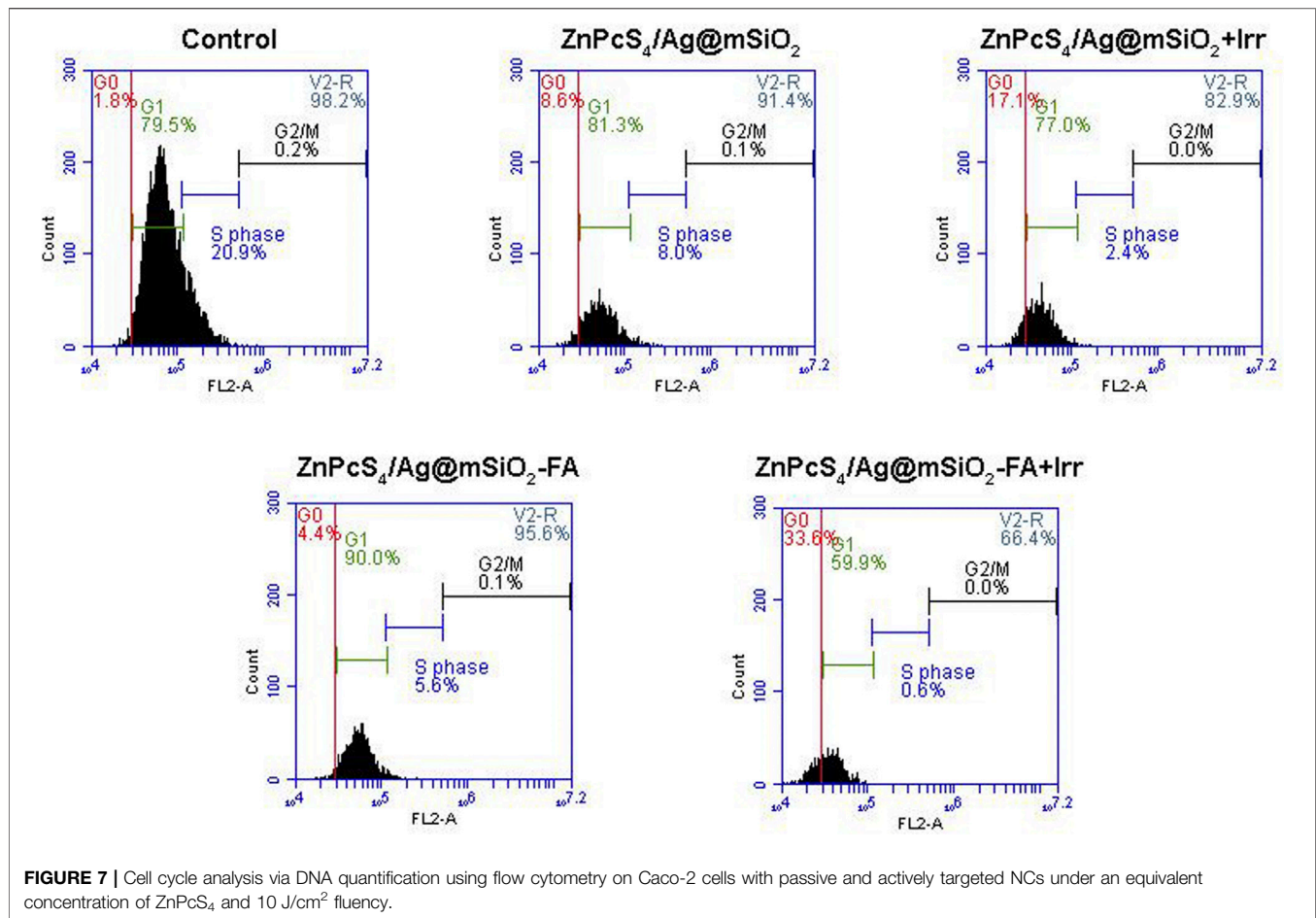
## 3.6 Flow Cytometry Cell Cycle Analysis

To clarify the antiproliferative effect of the passive and active NCs, cell cycle analysis was carried out by quantifying cellular DNA via flow cytometry. An equivalent concentration of ZnPcS$_4$ (0.125 μM, IC$_{50}$) and 10 J/cm$^2$ fluency were chosen for the PDT treatment of Caco-2 cells. Cells mature and copy their DNA at the G1 and S phases, respectively, while the cells start to divide and undergo mitoses at the G2/M phase. Additionally, the G0 phase indicates cell cycle arrest or cell death which can be used to elaborate on the PDT effect of the NCs. As demonstrated in **Figure 7**, the cells are predominately in the G1 phase in the control and the NCs groups with no irradiation, whereas the PDT-treated cells with the passive and actively targeted NCs entered the G0 phase, which was correspondingly accompanied by a notable decrease in the S phase compared to the control cells. Furthermore, the cells treated with the actively targeted ZnPcS$_4$/Ag@mSiO$_2$-FA NC showed greater cell cycle arrest at the G0 phase compared to the passive targeted ZnPcS$_4$/Ag@mSiO$_2$ NC. These results suggest that the NCs under PDT treatment could induce cell cycle arrest at the G0 phase, thereby interfering with the cell cycle progression into the G1 and S phases, which may be associated with the inhibition of proliferation.

## 4 CONCLUSION

The present results demonstrate that a nanotechnology-based strategy with FA-conjugated NPs efficiently targets cancer cells for photodynamic therapy of Caco-2 cells. In this regard, core/shell Ag@mSiO$_2$ NPs were synthesized and loaded with ZnPcS$_4$ PS. FA was also decorated onto the surface of the NC to overexpress folate receptors and enhance the active targeting PDT. Cytotoxicity and viability experiments in Caco-2 cancer cells noted that the drug-mediated toxicity of the ZnPcS$_4$/Ag@mSiO$_2$-FA NC under 674 nm laser irradiation was better than the passive NC and free PS, while its adverse effect on WS1 normal cells seemed to be negligible. The analysis of apoptotic and necrotic cells by flow cytometry elucidated that apoptosis was the major pathway of cell death with a 52.4% ± 3.5** apoptotic ratio for the cells treated with the ZnPcS$_4$/Ag@mSiO$_2$-FA-PDT. Additionally, the preliminary findings in this study showed that the actively targeted NC induced G0 cell cycle arrest. Possibly, the ZnPcS$_4$/Ag@mSiO$_2$-FA NC can be applied as a promising theranostics PDT for effective cancer therapy. However, due to the preliminary nature of the study, further experiments on the detection of the expression of proteins associated with the apoptotic pathway after treatment with ZnPcS$_4$/Ag@mSiO$_2$-FA NC-PDT are to be investigated.

# DATA AVAILABILITY STATEMENT

The datasets generated during and/or analyzed during the current study are available from the corresponding author upon request.

# AUTHOR CONTRIBUTIONS

HM: study design, acquisition of data, analysis and interpretation of data, and the drafting and revision of the article. NWNS: acquisition of data and revision of the article. HA: revision of the article and final approval of the article. All authors have read and agreed to the published version of the manuscript.

# REFERENCES

Agostinis, P., Berg, K., Cengel, K. A., Foster, T. H., Girotti, A. W., Gollnick, S. O., et al. (2011). Photodynamic Therapy of Cancer: an Update. *CA A Cancer J. Clin.* 61 (4), 250–281. doi:10.3322/caac.20114

Almeida, R. D., Manadas, B. J., Carvalho, A. P., and Duarte, C. B. (2004). Intracellular Signaling Mechanisms in Photodynamic Therapy. *Biochim, Biophys. Acta (BBA) - Rev. Cancer* 1704 (2), 59–86. doi:10.1016/j.bbcan.2004.05.003

Banfi, S., Caruso, E., Buccafurni, L., Ravizza, R., Gariboldi, M., and Monti, E. (2007). Zinc Phthalocyanines-Mediated Photodynamic Therapy Induces Cell Death in Adenocarcinoma Cells. *J. Organomet. Chem.* 692 (6), 1269–1276. doi:10.1016/j.jorganchem.2006.11.028

Bretin, L., Pinon, A., Bouramtane, S., Ouk, C., Richard, L., Perrin, M. L., et al. (2019). Photodynamic Therapy Activity of New Porphyrin-Xylan-Coated Silica Nanoparticles in Human Colorectal Cancer. *Cancers (Basel)* 11 (10), 1474. doi:10.3390/cancers11101474

Danaei, M., Dehghankhold, M., Ataei, S., Hasanzadeh Davarani, F., Javanmard, R., Dokhani, A., et al. (2018). Impact of Particle Size and Polydispersity Index on the Clinical Applications of Lipidic Nanocarrier Systems. *Pharmaceutics* 10 (2), 57. doi:10.3390/pharmaceutics10020057

Dhami, S., Cosa, J. J., Bishop, S. M., and Phillips, D. (1996). Photophysical Characterization of Sulfonated Aluminum Phthalocyanines in a Cationic Reversed Micellar System. *Langmuir* 12 (2), 293–300. doi:10.1021/la950968m

El-Hammadi, M. M., Delgado, Á. V., Melguizo, C., Prados, J. C., and Arias, J. L. (2017). Folic Acid-Decorated and PEGylated PLGA Nanoparticles for Improving the Antitumour Activity of 5-fluorouracil. *Int. J. Pharm.* 516 (1-2), 61–70. doi:10.1016/j.ijpharm.2016.11.012

Fife, J., Raniga, S., Hider, P. N., and Frizelle, F. A. (2011). Folic Acid Supplementation and Colorectal Cancer Risk: a Meta-analysis. *Colorectal Dis.* 13 (2), 132–137. doi:10.1111/j.1463-1318.2009.02089.x

Gantchev, T. G., van Lier, J. E., and Hunting, D. J. (2005). Molecular Models of Zinc Phthalocyanines: Semi-empirical Molecular Orbital Computations and Physicochemical Properties Studied by Molecular Mechanics Simulations. *Radiat. Phys. Chem.* 72 (2-3), 367–379. doi:10.1016/j.radphyschem.2004.06.012

Han, L., Wei, H., Tu, B., and Zhao, D. (2011). A Facile One-Pot Synthesis of Uniform Core-Shell Silver Nanoparticle@mesoporous Silica Nanospheres. *Chem. Commun.* 47 (30), 8536–8538. doi:10.1039/c1cc12718g

Hani, U., Honnavalli, Y. K., Begum, M. Y., Yasmin, S., Osmani, R. A. M., and Ansari, M. Y. (2021). Colorectal Cancer: A Comprehensive Review Based on the Novel Drug Delivery Systems Approach and its Management. *J. Drug Deliv. Sci. Technol.* 63, 102532. doi:10.1016/j.jddst.2021.102532

Hoener, B. S., Zhang, H., Heiderscheit, T. S., Kirchner, S. R., De Silva Indrasekara, A. S., Baiyasi, R., et al. (2017). Spectral Response of Plasmonic Gold Nanoparticles to Capacitive Charging: Morphology Effects. *J. Phys. Chem. Lett.* 8 (12), 2681–2688. doi:10.1021/acs.jpclett.7b00945

Huang, X., Jain, P. K., El-Sayed, I. H., and El-Sayed, M. A. (2008). Plasmonic Photothermal Therapy (PPTT) Using Gold Nanoparticles. *Lasers Med. Sci.* 23 (3), 217–228. doi:10.1007/s10103-007-0470-x

Huryn, D. M., Kornfilt, D. J. P., and Wipf, P. (2019). p97: an Emerging Target for Cancer, Neurodegenerative Diseases, and Viral Infections. *J. Med. Chem.* 63 (5), 1892–1907. doi:10.1021/acs.jmedchem.9b01318

Kievit, F. M., and Zhang, M. (2011). Cancer Nanotheranostics: Improving Imaging and Therapy by Targeted Delivery across Biological Barriers. *Adv. Mat.* 23 (36), H217–H247. doi:10.1002/adma.201102313

Kim, B., Han, G., Toley, B. J., Kim, C.-k., Rotello, V. M., and Forbes, N. S. (2010). Tuning Payload Delivery in Tumour Cylindroids Using Gold Nanoparticles. *Nat. Nanotech.* 5 (6), 465–472. doi:10.1038/nnano.2010.58

Krajczewski, J., Rucińska, K., Townley, H. E., and Kudelski, A. (2019). Role of Various Nanoparticles in Photodynamic Therapy and Detection Methods of Singlet Oxygen. *Photodiagn. Photodyn. Ther.* 26, 162–178. doi:10.1016/j.pdpdt.2019.03.016

Low, P. S., and Kularatne, S. A. (2009). Folate-Targeted Therapeutic and Imaging Agents for Cancer. *Curr. Opin. Chem. Biol.* 13 (3), 256–262. doi:10.1016/j.cbpa.2009.03.022

Lucky, S. S., Soo, K. C., and Zhang, Y. (2015). Nanoparticles in Photodynamic Therapy. *Chem. Rev.* 115 (4), 1990–2042. doi:10.1021/cr5004198

Melamed, J. R., Edelstein, R. S., and Day, E. S. (2015). Elucidating the Fundamental Mechanisms of Cell Death Triggered by Phototherapy. *ACS Nano* 9 (1), 6–11. doi:10.1021/acsnano.5b00021

Montaseri, H., Kruger, C. A., and Abrahamse, H. (2021). Targeted Photodynamic Therapy Using Alloyed Nanoparticle-Conjugated 5-Aminolevulinic Acid for Breast Cancer. *Pharmaceutics* 13 (9), 1375. doi:10.3390/pharmaceutics13091375

Porrang, S., Davaran, S., Rahemi, N., Allahyari, S., and Mostafavi, E. (2022). How Advancing Are Mesoporous Silica Nanoparticles? A Comprehensive Review of the Literature. *Int. J. Nanomed.* 17, 1803–1827. doi:10.2147/ijn.s353349

Portilho, F. A., Cavalcanti, C. E. d., Miranda-Vilela, A. L., Estevanato, L. L. C., Longo, J. P. F., Almeida Santos, M. d., et al. (2013). Antitumor Activity of Photodynamic Therapy Performed with Nanospheres Containing Zinc-Phthalocyanine. *J. Nanobiotechnol.* 11, 41. doi:10.1186/1477-3155-11-41

Sibata, C. H., Colussi, V. C., Oleinick, N. L., and Kinsella, T. J. (2000). Photodynamic Therapy: a New Concept in Medical Treatment. *Braz J. Med. Biol. Res.* 33 (8), 869–880. doi:10.1590/s0100-879x2000000800002

Simelane, N. W. N., Kruger, C. A., and Abrahamse, H. (2021). Targeted Nanoparticle Photodynamic Diagnosis and Therapy of Colorectal Cancer. *Int. J. Mol. Sci.* 22 (18), 9779. doi:10.3390/ijms22189779

Simioni, A. R., Martins, O. P., Lacava, Z. G. M., Azevedo, R. B., Lima, E. C. D., Lacava, B. M., et al. (2006). Cell Toxicity Studies of Albumin-Based Nanosized Magnetic Beads. *J. Nanosci. Nanotech.* 6 (8), 2413–2415. doi:10.1166/jnn.2006.511

Sudimack, J., and Lee, R. J. (2000). Targeted Drug Delivery via the Folate Receptor. *Adv. Drug Deliv. Rev.* 41 (2), 147–162. doi:10.1016/s0169-409x(99)00062-9

Wang, N., Cheng, X., Li, N., Wang, H., and Chen, H. (2019). Nanocarriers and Their Loading Strategies. *Adv. Healthc. Mat.* 8 (6), 1801002. doi:10.1002/adhm.201801002

Wang, Y., Yang, M., Qian, J., Xu, W., Wang, J., Hou, G., et al. (2019). Sequentially Self-Assembled Polysaccharide-Based Nanocomplexes for Combined Chemotherapy and Photodynamic Therapy of Breast Cancer. *Carbohydr. Polym.* 203, 203–213. doi:10.1016/j.carbpol.2018.09.035

Wijesiri, N., Yu, Z., Tang, H., and Zhang, P. (2018). Antifungal Photodynamic Inactivation against Dermatophyte Trichophyton Rubrum Using Nanoparticle-Based Hybrid Photosensitizers. *Photodiagn. Photodyn. Ther.* 23, 202–208. doi:10.1016/j.pdpdt.2018.06.019

Yang, M., Chen, T., Lau, W. S., Wang, Y., Tang, Q., Yang, Y., et al. (2009). Development of Polymer-encapsulated Metal Nanoparticles as Surface-enhanced Raman Scattering Probes. *Small* 5 (2), 198–202. doi:10.1002/smll.200800777

Zhao, B., Yin, J.-J., Bilski, P. J., Chignell, C. F., Roberts, J. E., and He, Y.-Y. (2009). Enhanced Photodynamic Efficacy towards Melanoma Cells by Encapsulation of Pc4 in Silica Nanoparticles. *Toxicol. Appl. Pharmacol.* 241 (2), 163–172. doi:10.1016/j.taap.2009.08.010